NTNU
Kunnskap for en bedre verden

Department of Engineering Cybernetics

TTK4550 - Specialization Project

Design and Control of a Spring-actuated Jumping Quadruped in Earth Gravity

Author:
Johannes Ihle
Daniel Rosmæl Skauge

Supervisor:
Prof. Dr. Kostas Alexis

Co-supervisor:
Jørgen Anker Olsen

Date

Abstract

This project report presents our specialization project, which is the design and control of a quadruped, spring-actuated, etc.

Here I am trying to cite [12].

Table of Contents

List of Figures iii

List of Tables iv

1 Introduction 1

1.1 Motivation . . . 1

1.2 Scope . . . 2

1.3 Related Work . . . 2

2 Theory 3

2.1 Actuator Modeling . . . 3

2.1.1 DC Motor Model . . . 3

2.1.2 BLDC Motor Model . . . 3

2.1.3 Gear Transmission Friction Model . . . 3

2.2 Spring Modeling . . . 4

2.3 Spring-Damper Systems . . . 4

2.4 Kinematics, Jacobians, and Virtual Work . . . 4

2.4.1 Robot Kinematics . . . 4

2.4.2 Jacobian Matrix . . . 5

2.4.3 Force/Torque Mapping . . . 5

2.5 Numerical Solvers . . . 6

3 Modeling and Simulation 6

3.1 Simscape . . . 6

3.2 Rigid Body Components of the Robot Model . . . 6

3.3 Rigid Body Masses and Inertias . . . 8

3.4 Elastic Components: Springs . . . 10

3.5 Motor Modeling . . . 10

3.6 Solver selection . . . 11

4 Robot Design 11

4.1 The Single Vertical Manipulator Jump Model . . . 11

4.2 Actuation Method Selection: Motors Only . . . 12

4.3 Actuation Method Selection: Motors and Torsional Spring . . . 14

4.4 Actuation Method Selection: Motors and Extension Spring . . . 15

5 Robot Hardware **15**

5.1 Torsional Spring Leg 15

5.2 Extension Spring Leg design 15

5.3 Motor Selection 16

6 Results **18**

6.1 Motor Only Jumps 18

6.2 Motor Only Jumps with Spring 18

6.3 Hip Motor Dimensioning Test 18

7 Discussion **18**

8 Conclusion and Future Work **18**

Bibliography **19**

Appendix **20**

A A06CLS V2 Website Information 20

B A20BHM Website Information 20

C A35CHM Motor Information 21

List of Figures

1 Torque-speed characteristics of a BLDC motor. TODO: Replace with an image that isn't stolen, and that we are allowed to use. 3

2 Illustration of a 3 link robotic link arm in $\mathbb{R}^2$ with n links. 5

3 A typical Simscape block diagram. 7

4 A visualization of the model in figure 3. 7

5 Naming conventions for the parts of the robot, as well as forwards direction definition. TODO: name spines 8

6 Angle conventions for the robot body. 9

7 Extension spring implementation in Simscape. As can be seen, the spring is connected between the appropriate points (output frames) of the thigh and shank spine, and in parallel to the knee motor model, which contains the knee joint. 10

8 Torque-speed characteristics of the motor. 11

9 The manipulator corresponding to a vertical one leg jump. 12

10 Vertical Paw velocity as a function of knee angle. 13

11 Knee speed until takeoff with A80BHP-H motor. 14

12 An overview of the leg CAD model with a torsional spring. 15

13 An overview of the CAD model of the leg design, but showing only the components that will be manufactured inhouse. Axel that will be threaded and screwed directly into the motor shaft, and lead directly into a ball bearing, is emphasized in red. . 16

14 Comparison of extension spring configurations: outside (left) and inside (right) the leg. 17

15 Commanded and actual hip joint angle achieved during the hip motor strength test simulation. 18

16 A06CLS V2 Motor Information (Curt) 20

17 A35CHM Motor Information 21

List of Tables

2 Mass and inertia properties of the rigid bodies in the robot model. A list of the Eurepus robot's electronics can be found in [1]. 9

3 Masses and dimensions used in the main body mass calculation. 10

4 Selected Motors 16

Abbreviations

Abbreviation	Description
AI	Artificial Intelligence
API	Application Programming Interface
CPU	Central Processing Unit
DRL	Deep Reinforcement Learning
EKF	Extended Kalman Filter
ESKF	Error State Kalman Filter
GNC	Guidance, Navigation, and Control
INS	Inertial Navigation System
ML	Machine Learning
MOOS	Mission Oriented Operating Suite
PPO	Proximal Policy Optimization
RL	Reinforcement Learning
USV	Unmanned Surface Vehicle

1 Introduction

1.1 Motivation

TODO: Shorten the below drastically, but mention the loss of traction in low g for wheeled robots, mentioned in the SpaceHopper paper.

The exploration of extraterrestrial environments represents one of the most demanding frontiers of robotic systems, requiring exceptional autonomy, resilience, and adaptability to navigate complex and unpredictable terrain. On Mars, wheeled rovers have proven their utility, with six successful deployments to date [17], robots like Axel [7] and Reachbot [8] have also been designed, tailored towards specific tasks. One such task that has received much attention in recent years, is the exploration of potential Martian and Lunar lava tubes [2]. These tubes are hollow caverns hypothesized to exist beneath the surface of Mars and the Moon, formed by ancient lava flows. They are of particular interest to astrobiologists and planetary scientists, as they could provide shelter from cosmic radiation and micrometeorites, as well as stable temperatures and access to subsurface water ice [2].

The exploration of such lava tubes present a unique challenge to robotic systems, as they are believed to be characterized by rough, uneven terrain, sharp rocks, and steep slopes. This could present a challenge to traditional wheeled rovers. Further, the motion of wheeled robots is limited to the ground plane, and thus, inherently, they do not utilize the lower gravity of extraterrestrial objects such as asteroids, the Moon and Mars. Jumping quadrupeds, on the other hand, inherently utilize the lower gravity of such objects, and in low earth gravity could potentially jump to heights of several meters TODO: CITE. This could allow them to traverse obstacles that would be insurmountable to wheeled rovers, such as steep slopes, large rocks, and gaps in the terrain.

While recent years have seen great progress in the development of quadruped robots, most quadrupeds still struggle with jumping in earth gravity TODO: CITE. Since, additionally, low gravity environments are very hard to replicate on earth, it is difficult to test hardware and control algorithms intended for low gravity jumping quadrupeds. Jumping also includes high velocity impacts, making damage to the often expensive hardware likely. This motivates the main goal of this project, which is to develop a design for a small, lightweight, and low-cost jumping quadruped robot. The robot's low weight is intended to reduce the risk of damage during testing, and the low cost to make it more accessible to researchers, as well as reduce the cost of potential damage. Special emphasis is placed on being able to jump long distances, without losing the general utility of the quadruped form factor, such as the ability to walk on rough terrains, flexibly adjust body pose, and potentially carry scientific payloads.

1.2 Scope

As described in the Motivation section, section 1.1, the main goal of this project is to develop a design for a small, lightweight, and low-cost jumping quadruped robot. The work presented in this report is part of a specialization project, TTK4550 - Engineering Cybernetics, Specialization Project TODO: CITE, pursued at the Norwegian University of Science and Technology (NTNU), as a preparation for a master's thesis. So while the scope of the specialization project is limited to the development of a design, the overall goal is for the design to be used as the basis for a master's thesis, where the robot will be built and tested. The master's thesis will also include the development of control algorithms for the robot, which is not included in this report.

More precisely, the scope of this project is limited to the following:

- Developing a simplified simulation for the robot in MATLAB/Simulink, to be used for verification and evaluation of various design choices.
- Choosing a specific method of actuation, such as motors, parallel torsional springs, parallel extension springs, or a combination of these.
- Identifying key hardware components, such as motors and springs.
- Designing a CAD model for a single leg of the robot. The leg must adhere to geometric and mechanical constraints such as:
  - Accommodating chosen springs and motors.
  - Being easily manufacturable using 3D printing and machining TODO: WHAT?
  - Sturdiness, ie. being able to withstand the forces and impacts of jumping.

1.3 Related Work

The problem of robotic jumping in earth and low gravity environments has been studied by several researchers, with various approaches taken. One unique example is the Olympus robot [9] [10] developed by NTNU's ARL (Autonomous Robots lab), which uses a 5-bar linkage spring assisted leg to jump. The robot weighs TODO kg, is capable of jumping to heights of up to TODO meters in earth gravity, and has been tested in simulated low gravity environments. Another example is the 600g robot RAVEN (Robotic Avian-inspired Vehicle for multiple ENvironments) [13] developed at EPFL, which uses its bird-inspired 2 DOF multifunctional legs to jump rapidly into flight, walk on the ground, and hop over obstacles and gaps similar to the multimodal locomotion of birds. Notable for RAVEN is its geared BLDC motors, which wind up embedded torsional springs, which then assist in jumping. Apart from the different topology of the legs and springs, the concept is quite similar to that of Olympus. The RAVEN robot can jump TODO (26 cm) cm in earth gravity. A third example is the Grillo robot [11], which weighs 15g and takes of at velocities of about 30 body lengths per second, ie. 1.5m/s.

2 Theory

2.1 Actuator Modeling

2.1.1 DC Motor Model

2.1.2 BLDC Motor Model

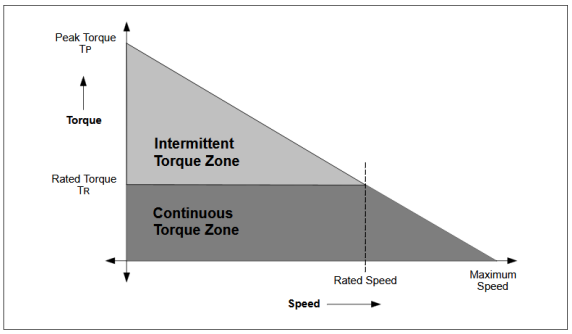

Figure 1: Torque-speed characteristics of a BLDC motor. TODO: Replace with an image that isn't stolen, and that we are allowed to use.

2.1.3 Gear Transmission Friction Model

Although electric motors for robotics are available for a wide power range, they are often too high speed and low power to do any useful work. For this reason, it is often necessary to use a gear transmission to increase the torque and reduce the speed of the motor.

In the presence of a geared transmission, assuming no power loss, the output torque and velocity of a geared motor are given by equation 1 and equation 2, respectively, where N is the gear ratio, τ_{in} is the input torque, τ_{out} is the output torque, w_{in} is the input velocity, and w_{out} is the output velocity [5].

$$w_{out} = \frac{w_{in}}{N} \tag{1}$$

$$\tau_{out} = N\tau_{in} \tag{2}$$

In reality, however, there is always some power loss in the transmission. A common way to model this is to use friction model consisting of a viscous friction term and a Coulomb friction term [5]. The viscous friction term is proportional to the velocity of the transmission, and the Coulomb friction term is a constant friction torque that must be overcome before the transmission starts moving. The total friction torque is the sum of these two terms, as seen in equation 3. It is also possible to drop one or the other of these terms, depending on the application [5].

$$\tau_{friction} = b_{viscous}\dot{\theta} + b_{coulomb}\text{sign}(\dot{\theta}) \tag{3}$$

In addition to friction, heavily gearing motors can lead to a very high apparent rotor inertia. If one looks at equation 4, it is clear that the apparent rotor inertia is proportional to the square of the gear ratio [5]. This can lead to a very high apparent rotor inertia, which can often be problematic to robotic applications. This is especially the case for cases with contact forces, as the high apparent rotor inertia can lead to very stiff and damaging collisions [16].

$$K = \frac{1}{2}I_{rotor}(G\dot{\theta})^2 = \frac{1}{2}I_{rotor}G^2(\dot{\theta})^2 = \frac{1}{2}I_{apparent}(\dot{\theta})^2 \tag{4}$$

2.2 Spring Modeling

Springs are mechanical devices that store and release energy when subjected to displacement. There are two main types of springs: extension springs and torsion springs.

Extension springs are designed to operate with a tension load, meaning they extend as the load is applied. The force exerted by an extension spring is proportional to the displacement from its equilibrium position, following Hooke's Law, which is given by:

$$F = -kx \tag{5}$$

where F is the force exerted by the spring, k is the spring constant, and x is the displacement from the equilibrium position. The potential energy stored in an extension spring is given by:

$$U = \frac{1}{2}kx^2 \tag{6}$$

Torsion springs, on the other hand, are designed to operate with a rotational or twisting load. They exert a torque that is proportional to the angular displacement from their equilibrium position. The torque generated by a torsion spring is given by:

$$\tau = -k\theta \tag{7}$$

where τ is the torque, k is the torsion spring constant, and θ is the angular displacement. The potential energy stored in a torsion spring is given by:

$$U = \frac{1}{2}k\theta^2 \tag{8}$$

Both types of springs are widely used in various mechanical systems to provide force or torque, absorb shock, and store energy.

2.3 Spring-Damper Systems

2.4 Kinematics, Jacobians, and Virtual Work

2.4.1 Robot Kinematics

Consider a robotic link arm existing in $\mathbb{R}^2$ consisting of n links, each with a length l_i and a joint angle q_i. The position of the end-effector is given by the vector $\mathbf{x} = [x, y]^T$, where x and y are the coordinates of the end-effector in the global coordinate system. Using simple trigonometry, the position of the end-effector can be expressed as a function of the joint angles and link lengths as seen in equation 9. Axes and joint angles corresponding to the expression in equation 9 can be seen in figure 2.

$$\mathbf{x} = \begin{bmatrix} x \\ y \end{bmatrix} = \begin{bmatrix} \sum_{i=1}^{n} l_i \cos(q_i) \\ \sum_{i=1}^{n} l_i \sin(q_i) \end{bmatrix} \tag{9}$$

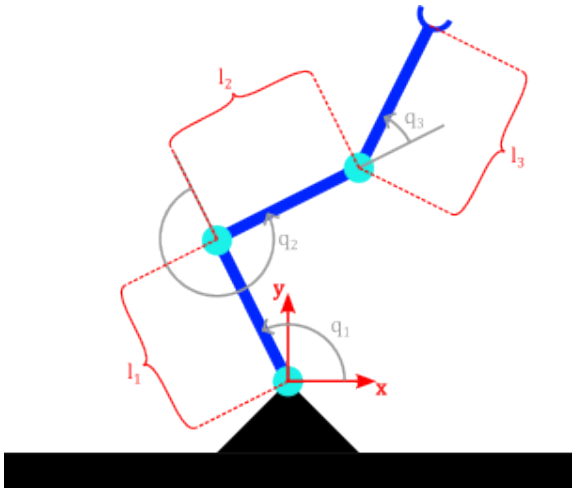

Figure 2: Illustration of a 3 link robotic link arm in $\mathbb{R}^2$ with n links.

2.4.2 Jacobian Matrix

As described in section 2.4.1, the position of the end-effector can be expressed as a function of the joint angles and link lengths. In robotics, it is often useful to express the relationship between infinitesimal changes in the joint angles and the resulting change in the end-effector position. As can be seen in equation 10, infinitesimal changes in variables δy and δx can be described by means of the partial derivative [3]. If this is compared to the definition of the jacobian in equation 11, it is clear that the jacobian matrix $\mathbf{J}$ can be used to map infinitesimal changes in joint angles to changes in the end-effector position, as illustrated in equation 12. The limit of an infinitesimal change over an infinitesimal time interval is a derivative, and thus by dividing each side in equation 12 by δt, one arrives at the expression in equation 13, by which the jacobian can be used to map joint velocities to end-effector velocities.

$$\delta y = \frac{\partial y}{\partial x}\delta x \tag{10}$$

$$\mathbf{J} = \begin{bmatrix} \frac{\partial x}{\partial q_1} & \frac{\partial x}{\partial q_2} & \cdots & \frac{\partial x}{\partial q_n} \\ \frac{\partial y}{\partial q_1} & \frac{\partial y}{\partial q_2} & \cdots & \frac{\partial y}{\partial q_n} \end{bmatrix} \tag{11}$$

$$\delta \mathbf{x} = \mathbf{J}\delta \mathbf{q} \tag{12}$$

$$\dot{\mathbf{x}} = \mathbf{J}\dot{\mathbf{q}} \tag{13}$$

2.4.3 Force/Torque Mapping

Consider a general robotic manipulator, such as the one illustrated in figure 2, but with an arbitrary amount, n, of joints and links. Using the principle of conservation of power, one arrives at the formulation found in equation 14.

$$\text{power at the joints} = (\text{power to move the robot}) + (\text{power at the end-effector}) \tag{14}$$

As the power used to move the robot approaches zero,

Finally found northwestern book that says what I need: [5].

Consider a robotic manipulator with n joints, each with a joint angle q_i and a joint torque τ_i. The position of the end effector for such a system is given by equation 9, and thus the formula in equation 13 can be used to map joint velocities to end effector velocities.

$$\tau = J^T F \tag{15}$$

2.5 Numerical Solvers

Although a detailed review of numerical solvers and the associated theory is beyond the scope of this theory section, it is worth mentioning that numerical simulation of contact dynamics is particularly challenging. This is due to the discontinuities and high-frequency events that occur during contact. These dynamics often require the use of stiff solvers to accurately capture the rapid changes in forces and velocities [4][14]. Stiff solvers are designed to handle problems with widely varying timescales, ensuring stability and accuracy in the simulation of contact events. Without the use of stiff solvers, simulations can become unstable or fail to converge, leading to inaccurate results. Examples of stiff solvers include the well known ode15s and ode23s solvers in MATLAB, which are specifically designed to handle stiff ordinary differential equations [15].

3 Modeling and Simulation

For the purpose of doing design verification and optimization, a simplified model of the robot was created. The model was created in Simscape, a physical modeling toolbox integrated with MATLAB/Simulink.

3.1 Simscape

Simscape is a simulation tool that allows you to rapidly create models of physical systems within Mathworks' MATLAB/Simulink environment. With Simscape, physical systems are built by interconnecting blocks representing physical components, such as rigid bodies, joints and springs in a block diagram. The blocks are parameterized by physical properties, such as mass, inertia, and damping. Simscape automatically generates the equations of motion for the system, which can be solved numerically to simulate the system's behavior. Like you can do with Simulink without Simscape, you can also add ordinary Simulink blocks, including Matlab Function blocks, to the model. Simscape is also compatible with Simulink's multiple numerical solvers, such as ode15s, ode45, and ode23s (TODO? Is it ode23t?).

An example of a typical SimScape block diagram can be found in figure 3. A visualization of the corresponding model can be seen in figure 4. As one can see, each element in a block diagram is typically either a rigid body, or joints connecting the various rigid bodies. Since a given body has multiple possible locations that a joint could be connected to, as well as axes it can act on, blocks can export different frames, with different origins and orientations, depending on the desired position and orientation of the joint. For example, for a block representing the robotic equivalent of a thigh, natural output frames would be the ones with origins at the top and bottom of the thigh, with a select axis aligned with the desired knee or hip axis of rotation. TODO: We want to use something other than the tutorial here, but our robot model is too split into submodels of submodels, so it loses the intuition you get from a "flatter" model. Will fix later.

3.2 Rigid Body Components of the Robot Model

Since the purpose of the Simscape model is not to facilitate the development of a complicated full degree of freedom feedback controller, nor to optimize every small detail of the design, a simplified model was selected. This model consists of a main body with four legs, each of which with two

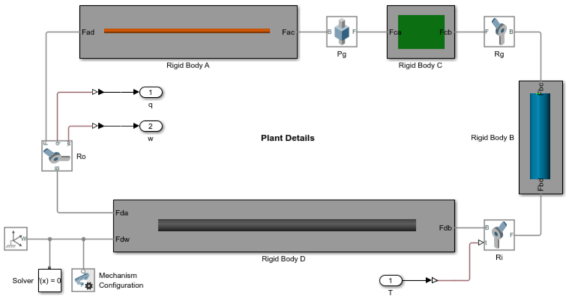

Figure 3: A typical Simscape block diagram.

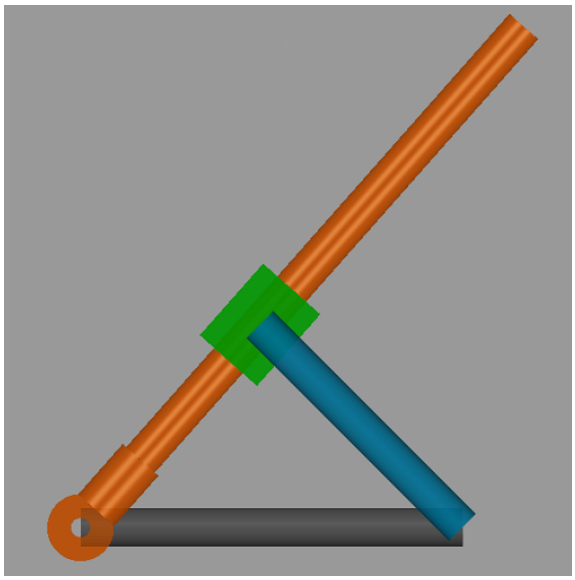

Figure 4: A visualization of the model in figure 3.

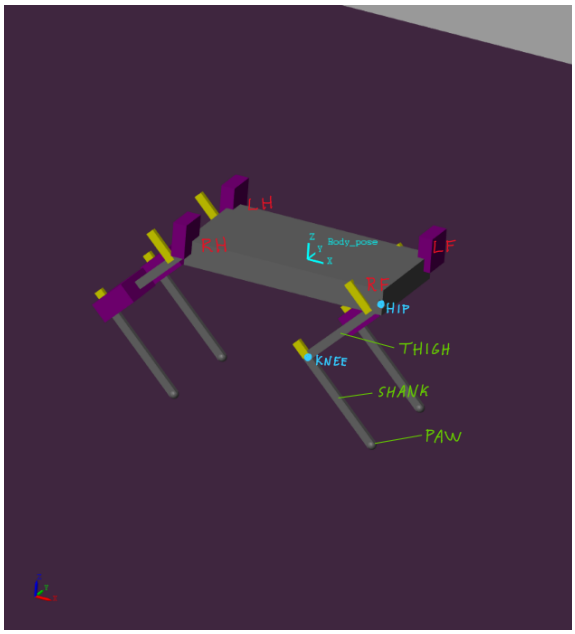

Figure 5: Naming conventions for the parts of the robot, as well as forwards direction definition. TODO: name spines

degrees of freedom. A visualization of the model, as well as an overview of the body's naming conventions can be found in figure 5. An overview of the body's angle conventions can be found in figure 6. Note the absence of a hip abduction/adduction joint. This is because the model's main purpose is to verify the design for jumping in the sagittal (forward-backward and upwards-downwards) plane, and the hip abduction/adduction joint is not necessary for this purpose.

Regarding the naming conventions presented in figure 5, note especially the naming of the different legs corresponding to location on the body, namely RH (Right Hind), RF (Right Front), LH (Left Hind), and LF (Left Front). Note also the naming of the joints hip (HIP) and knee (KNEE). If you see the angle conventions in figure 6, you can see that the angles of these joints correspond to the angles θ_1 and θ_2 respectively. Note that an orientation of zero degrees for the hip joint corresponds to the leg pointing straight downwards, and an orientation of zero degrees for the knee joint corresponds to the shank pointing in the same direction as the thigh.

TODO: Add body coordsys in both figures? So I can explain that positive rotation for both sides corresponds to positive rotation about the body y axis in nominal position.

As can be seen in both figure 5 and figure 6, in addition to the main body and legs colored in grey, the robot model also contains large purple blocks. These blocks represent motor masses, and their mass can be adjusted to represent different motors.

3.3 Rigid Body Masses and Inertias

In Simscape, the mass and inertia properties of a rigid body can be specified by the user or automatically calculated based on the body's geometry and material properties. Hybrid solutions are also possible, where the user specifies some properties and Simscape calculates the rest [6].

In the case of this model, a summary of the origin of the mass and inertia properties of the rigid bodies can be found in table 2. Exceptions are the properties of the main body and the paws, which will be specified in more detail in the two next paragraphs. For the parts whose mass and inertia are calculated by the geometry, this geometry will be specified in detail whenever the model is used, for example, section ref: TODO, the link-length optimization section, will specify the geometry assumed during the optimization.

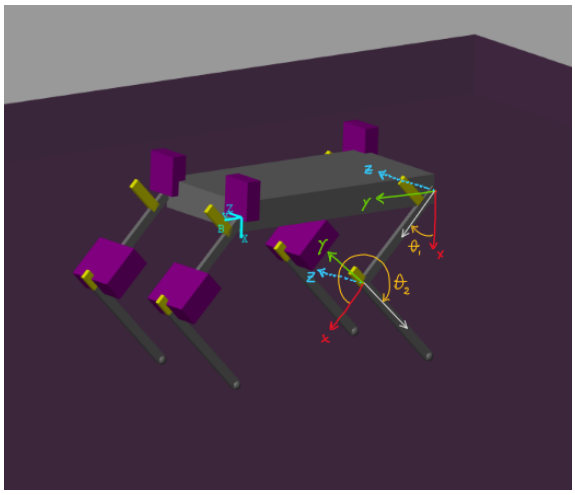

Figure 6: Angle conventions for the robot body.

Component	Mass	Density (kg/m^3)	Inertia	Geometry
Main Body	See section 3.3	See section 3.3	See section 3.3	Rectangular Prism
Thigh	From geometry	2700 (Aluminium 6061)	From geometry	Rectangular Prism
Shank	From Geometry	2700 (Aluminium 6061)	From Geometry	Rectangular Prism
Law	From Geometry	2700 (Aluminium 6061)	From Geometry	Rectangular Prism
Hip Motor	Actual motor mass	From Geometry	From Geometry	Rectangular Prism
Knee Motor	Actual motor mass	From Geometry	From Geometry	Rectangular Prism
Thigh Spine	From Geometry	2700 (Aluminium 6061)	From Geometry	Rectangular Prism
Shank Spine	From Geometry	2700 (Aluminium 6061)	From Geometry	Rectangular Prism
Paw	See section 3.3	See section 3.3	See section 3.3	Sphere

Table 2: Mass and inertia properties of the rigid bodies in the robot model. A list of the Eurepus robot's electronics can be found in [1].

The mass properties of the main body are based on the hardware components used by the Eurepus robot constructed by Maurer and El Agroudi [1]. Since early in the design process a rough estimate was needed for the robot body mass, and it seemed likely that the electronic solution, apart from the motors, would be similar to the Eurepus robot, an approximate mass of the main body was calculated based on the mass of some of the Eurepus robot's electronics plus an approximate amount of Nylon body material, four motors, and a random chosen microcontroller (MCU) mass. The formula used for the approximate of the main body mass can be found in equations 16 to 18. The masses corresponding to variables in equations 16 to 18 can be found in table 3. The motor mass chosen in table 3 corresponds to the mass of the agfrc A20BHM motor, this motor was chosen because it is unlikely that the hip abduction/adduction motor will be any heavier than this, for details, see section 4 or robot hardware? TODO.

The geometrical, mass and inertia properties of the paws differ based on which of two scenarios we intend to simulate. The first scenario is the normal jumping scenario, in which the paw mass is simply set to 1000 kg/m^3, though choosing the actual density of rubber would maybe be more appropriate. The dimensions of the paw are in this scenario simply chosen so that the diameter coincides exactly with max(shank width, shank height). The second scenario was meant to test the leg motor's potential ability to do in air attitude stabilization like done in [1]. This scenario will be described in more detail in section TODO.

$$m_{plate} = \rho_{nylon} \cdot V_{plate} = \rho_{nylon} \cdot l_{plate} \cdot w_{plate} \cdot h_{plate} \tag{16}$$

$$m_{\text{eurepus\_electronics}} = m_{\text{battery}} + m_{\text{I2C}} + 12 \cdot m_{\text{ADC}} + m_{\text{PWM\_driver}} \tag{17}$$

Variable	Description	Value
ρ_{nylon}	Density of Nylon	1520 kg/m^3
l_{plate}	Length of the plate	10 cm
w_{plate}	Width of the plate	6 cm
h_{plate}	Height of the plate	1.67 cm
m_{battery}	Mass of the battery	27 g
m_{motor}	Mass of one motor	20 g
m_{I2C}	Mass of the I2C module	5.1 g
m_{ADC}	Mass of one ADC module	2.4 g
$m_{\text{PWM\_driver}}$	Mass of the PWM driver	8.5 g
m_{MCU}	Approximate mass of some microcontroller	30 g
$m_{\text{main\_body}}$	Resultant mass of the main body	332 g

Table 3: Masses and dimensions used in the main body mass calculation.

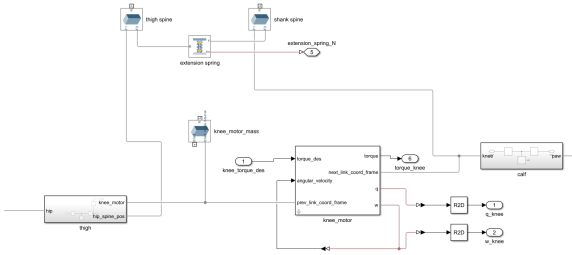

Figure 7: Extension spring implementation in Simscape. As can be seen, the spring is connected between the appropriate points (output frames) of the thigh and shank spine, and in parallel to the knee motor model, which contains the knee joint.

$$m_{\text{main\_body}} = m_{\text{plate}} + m_{\text{eurepus\_electronics}} + m_{MCU} + 4 \cdot m_{\text{motor}} \tag{18}$$

3.4 Elastic Components: Springs

In addition to the model's many rigid bodies, we also implemented two different forms of spring based passive actuation, namely:

- **A torsional spring** acting in parallel with the knee joint, as illustrated in figure TODO. This spring is at zero extension when the knee joint is at zero degrees, and applies a torque that is proportional to the knee joint angle, as covered in section 2.2.
- **An extension spring** acting in parallel with the knee joint, attached to the shank and thigh spine, as illustrated in TODO: add figure illustrating spines/add spine description in main body figure. The force generated by the extension spring is proportional to the displacement of the shank from the thigh, as covered in section 2.2.

The torsion spring was implemented in the model using Simscape's prismatic joint option to add spring stiffness. The extension spring, on the other hand, was connected in parallel to the joint using Simscape's natural block diagram functionality, as seen in figure 7.

3.5 Motor Modeling

To be able to more accurately judge the jumping capability of different motors, a motor model in the form of a torque speed curve was implemented. The BLDC torque-speed curve presented in figure 1 is characterized by four parameters, namely the stall torque, the operating torque, the

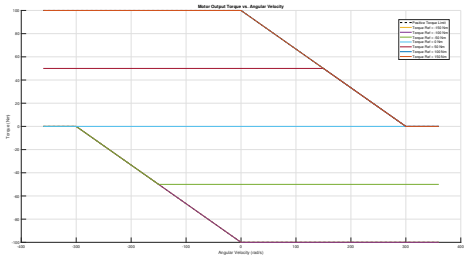

Figure 8: Torque-speed characteristics of the motor.

rated speed, and the maximum speed. Since motor suppliers contacted (primarily agf-rc and T-motor) were unable to provide most of the desired parameters, we chose a motor model with only two parameters, namely stall torque and maximum speed. The torque-speed model thus became a simple model where torque decreases linearly from stall torque, at speeds smaller than or equal to zero, to zero at speeds greater than or equal to maximum speed. The model is identical for negative velocities and torques, but with opposite signs. An example of the relation between desired torques and achieved torques for a given motor max speed can be seen in figure 8.

3.6 Solver selection

As described in section 2.2, the potential energy of a loaded spring can be easily calculated. Similarly, the potential energy due to gravity of a robot at the peak of a jump can also be determined. For the reasons discussed in section 2.5 we chose a stiff numerical solver, initially, we chose the ode15s solver. However, it was eventually observed that simulations using ode15s occasionally resulted in jump trajectories where the gravitational potential energy at the robot's peak height exceeded the combined potential energy of the four fully loaded springs by a factor of 2, even for jumps with only passive (spring) actuation. To address this inaccuracy, we experimented with different numerical solvers and ultimately selected the ode23s solver. This solver provided accurate simulations without artificially generating excess energy, and it performed efficiently.

4 Robot Design

This is where we explain "overall" design. It's motivation, etc. Also where we cover dimensioning, link-lengths, etc. We explain here our parameter sweep to find optimal design. We also explain here our kinematics-script that we used to derive the required stall-torque for our motor given springs and link-lengths.

4.1 The Single Vertical Manipulator Jump Model

In the absence of air resistance, which is negligible for a robot like this during a jumping maneuver like this, the factor that determines jumping distance is body velocity at takeoff. To keep things simple, in the following will be given an example where the sole goal is to maximize vertical jump height. Further, only a one leg robot with a 2 DOF leg with equal link lengths is considered.

For a robot such as the one described above, the position of the paw relative to the body can be described by the standard 2 link manipulator equation as seen in equation 19, in accordance with the theory in section 2.4.1. For this simple robot, it is assumed that the optimal jump is one where the body center of mass and paw position move in opposite directions, with velocities strictly along the up/down y axis. This example is illustrated in figure 9. As is obvious from the figure and from the kinematics, for such a jump $\theta_1 = -\frac{(\theta_2+\pi)}{2}$, and $\dot{\theta}_2 = -2\dot{\theta}_1$. If this is combined with the jacobian for the end effector, given in equation 4.1, one can plot the vertical velocity of the paw

as a function of the knee angle θ_2, this is shown in figure 10. This is done using the jacobian as in equation 13.

As can be seen in figure 10, the joint velocity of the leg much more readily translates to body velocity when the knee is crouched. Without giving a detailed derivation, the intuition meant to be gained from figure 10 is that how quickly the leg joints are accelerated can be just as important as the speed it is accelerated to. This has an important interpretation for the choice of motors, in the sense that, if a given motor is unable to accelerate the leg joints quickly enough, there is little sense in looking for a faster motor, unless it is also stronger.

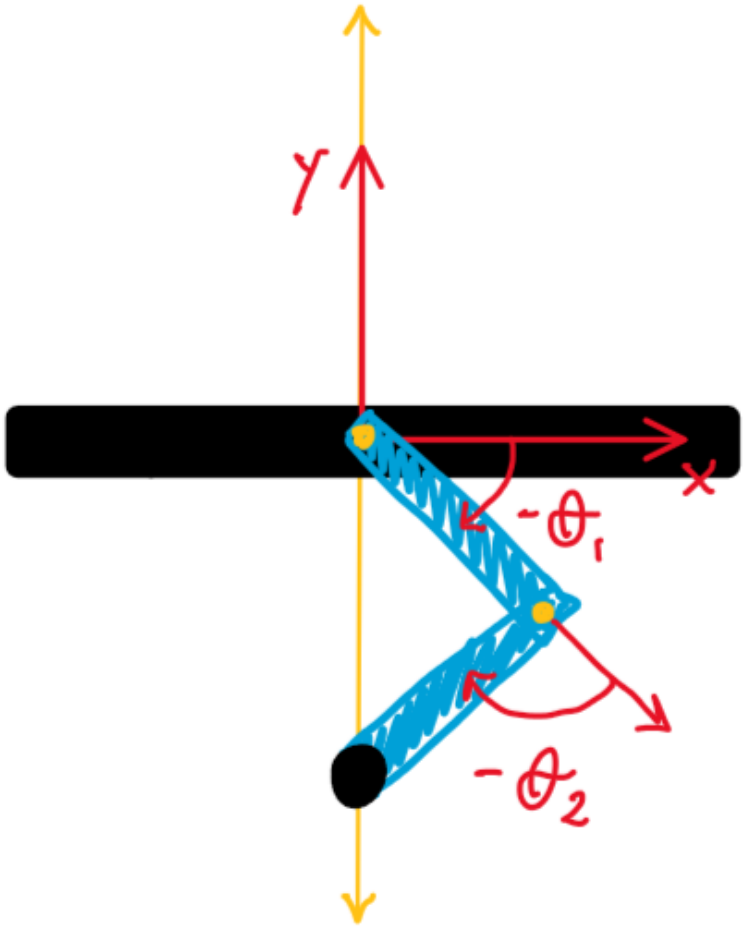

Figure 9: The manipulator corresponding to a vertical one leg jump.

$$\begin{aligned} x_{\text{end}} &= L_1 \cos(\theta_1) + L_2 \cos(\theta_1 + \theta_2) \\ y_{\text{end}} &= L_1 \sin(\theta_1) + L_2 \sin(\theta_1 + \theta_2) \end{aligned} \tag{19}$$

$$J = \begin{bmatrix} -L_1 \sin(\theta_1) - L_2 \sin(\theta_1 + \theta_2) & -L_2 \sin(\theta_1 + \theta_2) \\ L_1 \cos(\theta_1) + L_2 \cos(\theta_1 + \theta_2) & L_2 \cos(\theta_1 + \theta_2) \end{bmatrix}$$

4.2 Actuation Method Selection: Motors Only

Initially, experiments were done utilizing motors alone. Due to the need for a light and strong motor, initially a series of AGF-RC motors were looked at, due to their high torque to weight ratio. As covered in section 3.5, a motor model consisting of a stall torque and a max velocity,

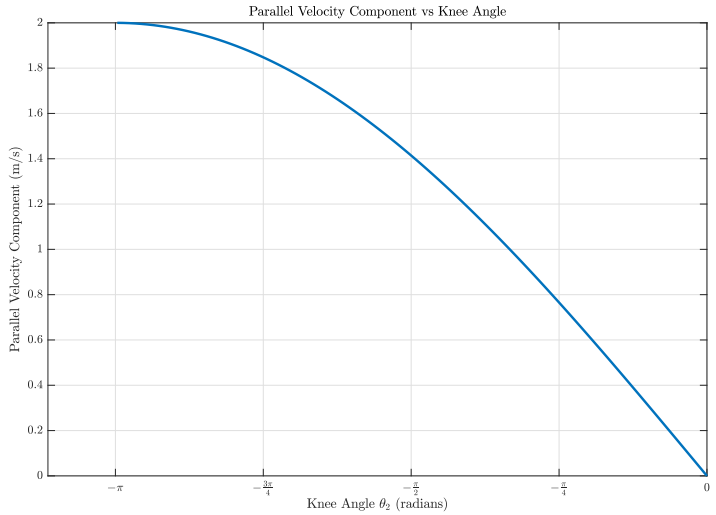

Figure 10: Vertical Paw velocity as a function of knee angle.

with a linear decrease in max torque between these two, was chosen. For the AGF-RC motors, their provided stall torque and operating speed were used as for the motor model parameters. Attempts were made to get more information about the motors' performance characteristics, but the supplier, AGF-RC, was unable to provide more detailed information. While extensive testing was done with various motors, the jumping performance was so far from acceptable that the idea was abandoned, and the full scope of the experiments are considered outside the scope of this report.

More details about the results of the motor only jumps can be found in section 6.1, but a brief overview of the reasoning involved will be given here. The most relevant of the motors chosen for these experiments was the A80BHP-H motor by AGFRC, which was chosen because it had both the highest stall torque and operating speed of all the AGF-RC motors. Attempts were made to identify motors with similar stall torques and operating speeds in the same weight range, but none were found. The experiments using the A80BHP-H were therefore, to a certain degree, considered an "optimistic estimate". Since no satisfactory results were achieved with the A80BHP-H motor, as discussed in section 6.1, it was decided to explore alternatives to motor-only actuation.

The tests with the A80BHP-H motor were done by providing the knee motors with reference torques equal to their max torque, with the motor model limiting the resultant torque to more realistic values. Meanwhile, the hip joints were actuated according to the control law seen in 23 to limit slipping. Despite the zero velocity/equilibria assumptions of equation 15, as presented in section 2.4.3, obviously not holding for this dynamic jumping scenario, very little slipping was observed in practice.

$$N = \text{Normal force} \tag{20}$$

$$\mu = \text{friction coefficient} = 0.8 \tag{21}$$

$$\tau_{\text{friction cone limit}} = J^T \begin{bmatrix} N\mu \\ 0 \end{bmatrix} \tag{22}$$

$$\max(|\tau_{knee}|) = \tau_{\text{friction cone limit}} \tag{23}$$

Using this control law, jumping for variously dimensioned robots were attempted. As covered in section 6.1, none of them were satisfactory. Tests were eventually terminated, as no and body link length configuration was capable of jumping satisfactorily. By satisfactorily, it is meant that the robot center of mass cleared the ground by a distance more than twice that of the leg length, ie., if the legs are 20cm long, the center of mass should clear the ground by at least 40cm.

For comparisons between this motor-only jumping and later spring+motor jumping, it is worth mentioning that the spring-motor jumping is done not with the A80BHP-H motors, but with weaker and slower motors, as well as with more realistic motor friction models. The reason the A80BHP-H motors were not used for the spring-motor jumping simulations, is that the motor supplier's website (AGF-RC) stated an operating travel range of 90 degrees. This was assumed to be correct, as other AGF-RC motors with stated operating ranges of 180 degrees have had actual mechanical limits of 220 degrees, so such a limitation was not considered out of the ordinary. Later consultations with the supplier's website revealed conflicting information regarding the operating range of the A80BHP-H motor, and direct contact with the supplier revealed that the motor is in fact not limited to 90 degrees of travel. For this reason, potential use of the A80BHP-H motor for the spring-motor jumping is discussed in the future work section, section 8. Despite this at the time believed limitation, the A80BHP-H motor was still used to ascertain the feasibility of motor-only jumping. This was done to provide a "best case scenario" for motor-only jumping, if results were poor for a motor better than any actual existing motor, it would be reasonable to assume that motor-only jumping is not feasible.

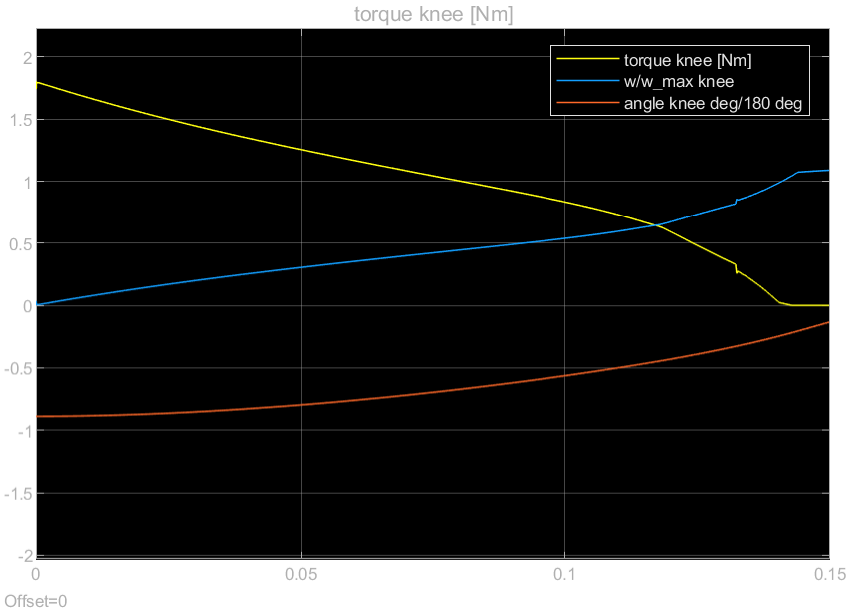

Figure 11: Knee speed until takeoff with A80BHP-H motor.

4.3 Actuation Method Selection: Motors and Torsional Spring

The next actuation method considered was to use a combination of motors and torsional springs, as this is the design we ended up choosing, a CAD model of this design can be seen in figure 12. With this design, the knee motors are used to compress the torsional springs, once the knee joint reaches a desired angle, ie. has stored the desired amount of energy, the motors are turned off, and the springs accelerate the legs joints quickly enough for the robot to take off. Results from simulations are presented in section 6.2, but in short, jumping performance was superior to that of the motor-only jumps. Tests were done both with and without motor friction. Due to the absence of known motor friction parameters, they were initially performed with assumed zero friction. Later tests, with motor friction parameters estimated based on physical experiments, are described in more detail in TODO, link length section, and results presented in TODO: link length results section.

4.4 Actuation Method Selection: Motors and Extension Spring

In addition to the torsional spring design, attempts were made to design a leg utilizing an extension spring. The resulting design is shown in figure 14. Although experiments akin to the ones done for torsional springs were done with comparable results, the extension spring design was ultimately abandoned. The reason for this was pure geometrical constraints, which are discussed in section 5.2. Because the extension spring design was abandoned, the details surrounding the extension spring simulations and simulation results are considered outside the scope of this report.

5 Robot Hardware

5.1 Torsional Spring Leg

Figure 12 shows the CAD model for the torsional spring leg design, including both knee and hip extension/flexion motor, as well as the hip adduction/abduction motor.

Figure 13 shows the components that are currently planned to manufacture in aluminum inhouse. The axel that will be threaded and screwed directly into the motor shaft, and lead directly into a ball bearing, is emphasized in red. Aluminum is planned to to its high strength-to-weight ratio, and the fact that it is easy to machine. Although many easily 3D-printable plastics are generally lighter, they are not as strong as aluminum. Due to the significant stiffness of the chosen spring, the leg has been designed so as to easily facilitate machining in aluminum. As the robot is manufactured, if 3D printable plastic is found to be sufficiently strong, appropriate parts will be 3D printed instead.

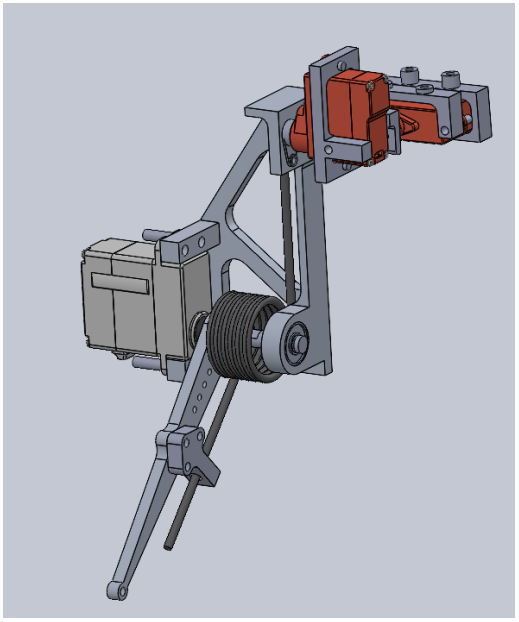

(a) Notice the bearing holding the knee-joint shaft in place. This is important to reduce the load the motor shaft suffers in directions other than the load direction.

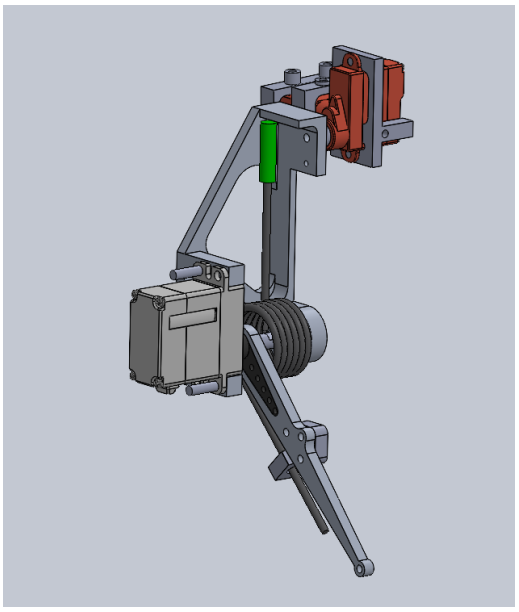

(b) As can be seen, there is a green plastic (PLA) holster where the spring is in contact with the leg, this is to reduce friction.

Figure 12: An overview of the leg CAD model with a torsional spring.

5.2 Extension Spring Leg design

The extension spring leg design is shown in figure 14. As can be seen in the figure, the current design is such that the extension spring will collide with the robot shank as the knee angle approaches

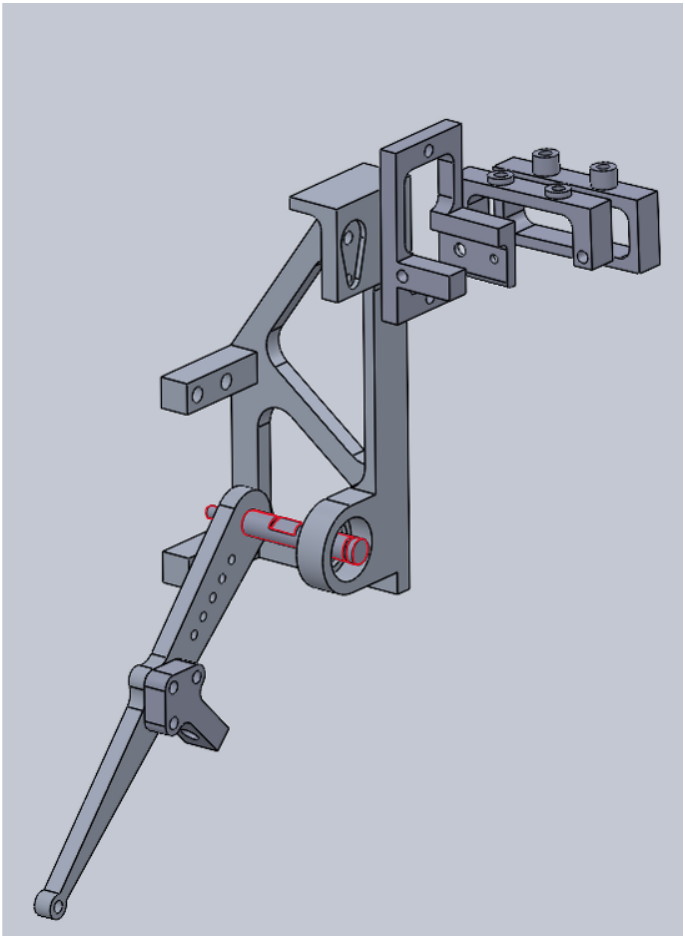

Figure 13: An overview of the CAD model of the leg design, but showing only the components that will be manufactured inhouse. Axel that will be threaded and screwed directly into the motor shaft, and lead directly into a ball bearing, is emphasized in red.

± 180 degrees. Despite efforts, no solutions were found for this problem, and this design direction was therefore abandoned. Among the suggested solutions was moving the shank-end attachment point of the spring in the inwards direction, thus allowing the extension spring to lie in parallel next to the shank when the leg is fully coiled. This would however introduce a significant moment arm acting directly on the motor shaft, and this design was therefore abandoned in favor of the torsional spring design.

5.3 Motor Selection

As discussed in section 4, the choice fell on AGF-RC motors due to their high torque to weight ratio, as well as our inability to find similarly fast motors of similar strength.

Our specific choice of motors can be found in table 4. Info about the specific motors can be found in appendices A to B.

Corresponding Joint	Motor Name
Knee flexion/extension	A20BHM
Hip flexion/extension	A06CLS V2
Hip adduction/abduction	A06CLS V2

Table 4: Selected Motors

The reason these motors in particular were chosen is the fact that no motors were found in a

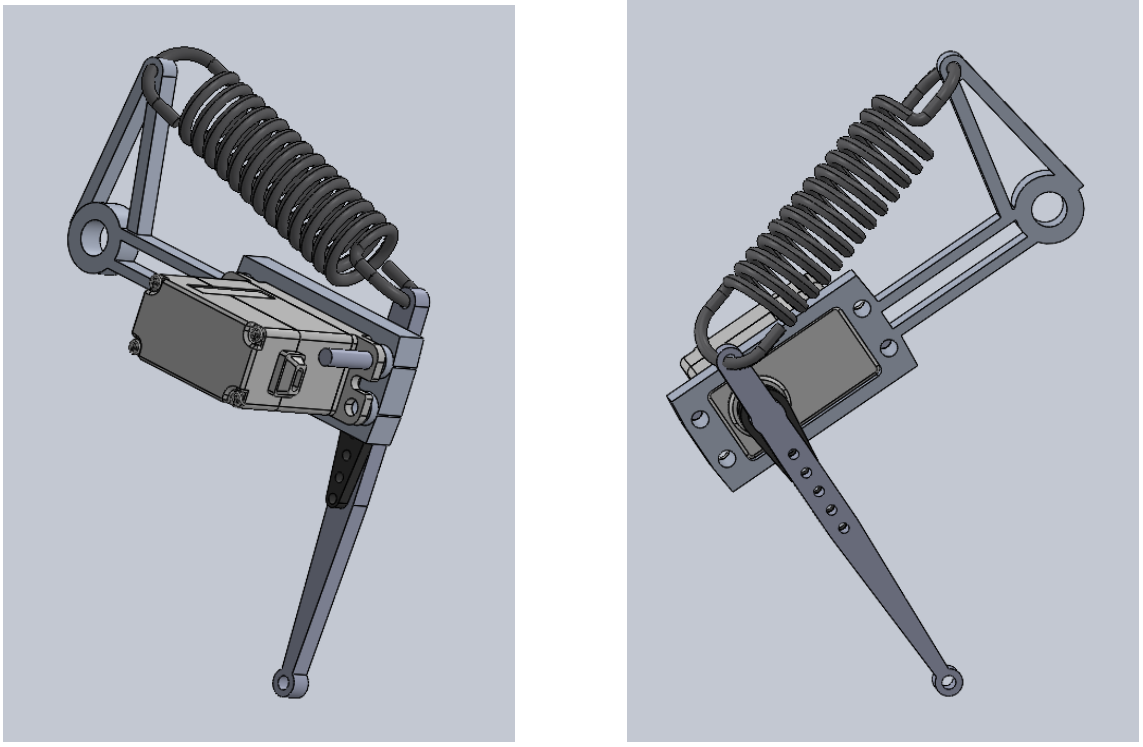

(a) The extension spring mounted on the outside of the leg. This configuration allows for easy adjustments and replacements.

(b) The extension spring mounted on the inside of the leg. This configuration provides a more compact design.

Figure 14: Comparison of extension spring configurations: outside (left) and inside (right) the leg.

similar weight class that could provide the same torque and speed. For example, if considering AGF-RC motors, the next motor, strength-wise, after the A20BHM motor, is the A35CHM motor, info about which can be found in appendix C. Despite being significantly heavier, the A35CHM motor is only marginally stronger than the A20BHM motor. The reasoning behind the choice of the A06CLS V2 motor was

6 Results

6.1 Motor Only Jumps

6.2 Motor Only Jumps with Spring

6.3 Hip Motor Dimensioning Test

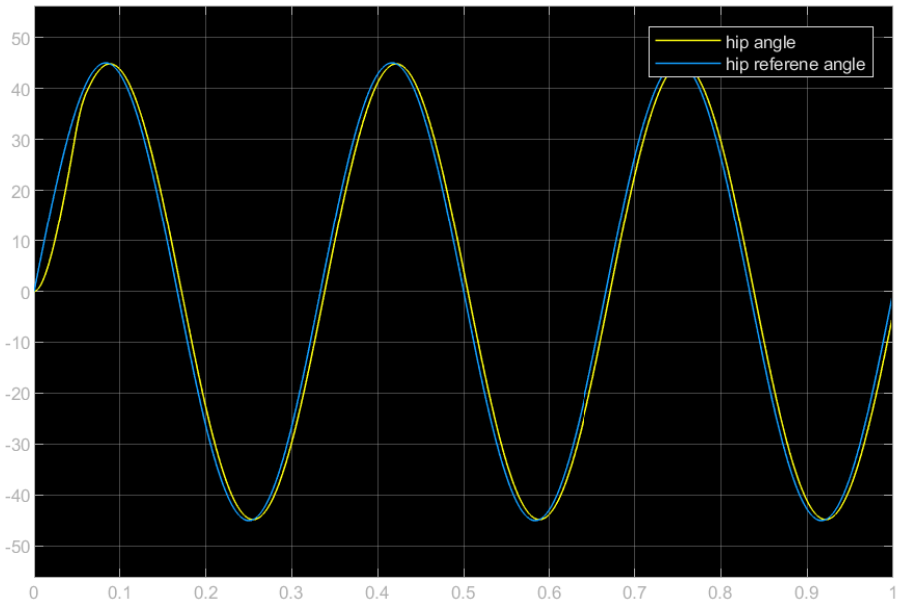

Figure 15: Commanded and actual hip joint angle achieved during the hip motor strength test simulation.

7 Discussion

8 Conclusion and Future Work

Bibliography

[1] Tarek El-Agroudi and Finn Gross Maurer. *In-Flight Attitude Control of a Quadruped in Low-Gravity Environments using Deep Reinforcement Learning*. 2024.

[2] Andrew Daga et al. *Lunar and Martian Lava Tube Exploration as Part of an Overall Scientific Survey*. White Paper submitted to the Planetary Sciences Decadal Survey 2013-2022. 2022.

[3] Olav Egeland and Jan Tommy Gravdahl. *Marine Cybernetics*. For ordering, visit http://www.marinecybernetics.com or contact info@marinecybernetics.com. Trondheim, Norway: Marine Cybernetics AS, 2002. URL: http://www.marinecybernetics.com.

[4] Ernst Hairer, Christian Lubich and Gerhard Wanner. *Geometric numerical integration: structure-preserving algorithms for ordinary differential equations*. Vol. 31. Springer Science & Business Media, 2006.

[5] Kevin M. Lynch and Frank C. Park. *MODERN ROBOTICS: MECHANICS, PLANNING, AND CONTROL*. Cambridge University Pres, 2017. ISBN: 978110715630.

[6] MathWorks. *Getting Started with Simscape*. https://se.mathworks.com/help/simscape/getting-started-with-simscape.html. Accessed: 2024-12-15. 2024.

[7] I. A. Nesnas et al. 'Axel and Duaxel Rovers for the Sustainable Exploration of Extreme Terrains'. In: *Journal of Field Robotics* 29.4 (2012), pp. 663–685.

[8] Stephanie Newdick et al. 'Designing ReachBot: System Design Process with a Case Study of a Martian Lava Tube Mission'. In: *2023 IEEE Aerospace Conference*. IEEE, 2023, pp. 1–9.

[9] Jørgen Anker Olsen and Kostas Alexis. 'Design and Experimental Verification of a Jumping Legged Robot for Martian Lava Tube Exploration'. In: *2023 21st International Conference on Advanced Robotics (ICAR)*. 2023, pp. 452–459. DOI: 10.1109/ICAR58858.2023.10406863.

[10] Jørgen Anker Olsen and Kostas Alexis. *Martian Lava Tube Exploration Using Jumping Legged Robots: A Concept Study*. 2023. arXiv: 2310.14876 [cs.RO]. URL: https://arxiv.org/abs/2310.14876.

[11] Umberto Scarfogliero, Cesare Stefanini and Paolo Dario. 'Design and Development of the Long-Jumping "Grillo" Mini Robot'. In: *Proceedings 2007 IEEE International Conference on Robotics and Automation*. 2007, pp. 467–472. DOI: 10.1109/ROBOT.2007.363830.

[12] John Schulman et al. *Proximal Policy Optimization Algorithms*. en. arXiv:1707.06347 [cs]. Aug. 2017. URL: http://arxiv.org/abs/1707.06347 (visited on 12th Nov. 2024).

[13] W.D. Shin, H.V. Phan, M.A. Daley et al. 'Fast ground-to-air transition with avian-inspired multifunctional legs'. In: *Nature* 636 (2024), pp. 86–91. DOI: 10.1038/s41586-024-08228-9.

[14] David E Stewart. 'Rigid-body dynamics with friction and impact'. In: *SIAM review* 42.1 (2000), pp. 3–39.

[15] Inc. The MathWorks. *MATLAB ODE Suite*. The MathWorks, Inc. Natick, MA, 2024. URL: https://www.mathworks.com/help/matlab/ref/ode15s.html.

[16] Patrick Wensing et al. 'Proprioceptive Actuator Design in the MIT Cheetah: Impact Mitigation and High-Bandwidth Physical Interaction for Dynamic Legged Robots'. In: *IEEE Transactions on Robotics* PP (Jan. 2017), pp. 1–14. DOI: 10.1109/TRO.2016.2640183.

[17] Mahboubeh Zarei and Robin Chhabra. 'Advancements in Autonomous Mobility of Planetary Wheeled Mobile Robots: A Review'. In: *Frontiers in Space Technologies* 3 (2022). ISSN: 2673-5075. DOI: 10.3389/frspt.2022.1080291.

Appendix

A A06CLS V2 Website Information

This information is taken from the website: https://www.agfrc.com/index.php?id=2666

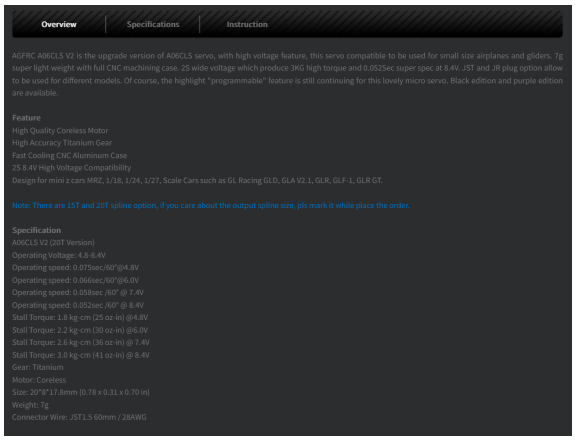

Figure 16: A06CLS V2 Motor Information (Curt)

B A20BHM Website Information

This information is taken from the website: https://www.agf-rc.com/agfrc-a20bhm-21g-high-speed-0068sec-114kg-progra
html

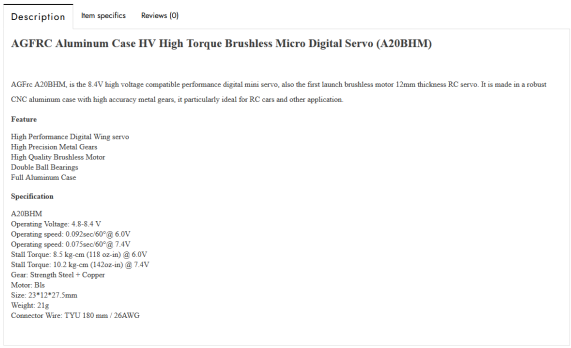

C A35CHM Motor Information

PRODUCT SPECIFICATION

A35CHM

Control System	Pulse width modulation control	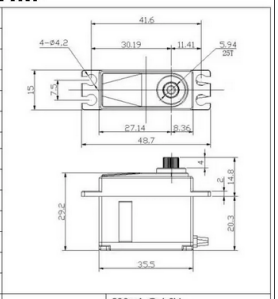	
Refresh Rate	333Hz		
Neutral Position	1520uS		
Signal Mode	Digital		
Dead band	2 uSec		
Operating Voltage	4.8V ~ 8.4V		
Operating Temperature	-15C°~+70C°		
Bearing	Dual Ball Bearing		
Mechanical Limit Angle	220°		
Size	35.5*15*29.2mm		
Net Weight	41g		
Wire	JR 180mm /22AGW		
Operating Travel	180°±10°		
Signal Range	500 to 2500 uSec		
Stall Torque	9.5 kg-cm (132 oz-in) @ 4.8V 10.5 kg-cm (146 oz-in) @ 6.0V 11.5 kg-cm (160 oz-in) @ 7.4V 12.5 kg-cm (174 oz-in) @ 8.4V	**Unload Current**	230mA @ 4.8V 300mA @ 6.0V 380mA @ 7.4V 420mA @ 8.4V
Operating Speed	0.145sec/ 60°@ 4.0V 0.125sec/60° @ 6.0V 0.095sec/60° @ 7.4V 0.085sec/60° @ 8.4V	**Loading Current**	2000mA @ 4.8V 2400mA @ 6.0V 2600mA @ 7.4V 2800mA @ 8.4V
Direction	☑ CCW ☐ CW		
Waterproof Level	☐ IP65 ☐ IP67		
Angle Sensor	☑Potentiometer ☐ Magnet Angle Sensor		
Motor Type	☐Brushless ☑Coreless ☐DC		
Motor Drive	☑FET Drive ☐IC Drive ☐Transistor Drive		
Programmable	☑ Yes ☐ No		
Gear Material	☐Strength Steel ☑Titanium ☐Copper ☐Plastic		
Horn Gear Spline	☑25T-φ5.92mm ☐25T-φ4.94mm ☐Other_____		
Case Material	☑AL6061T6 ☐AL+Plastic ☐Plastic		
Bearing Material	☑Metal ☐Plastic		
Horn Accessories	☐AL6061T6 ☑Plastic		
Wire Color	Negative: ☑ Black ☐Brown Positive: ☐ Black ☑Red Signal: ☐Grey ☑White ☐Orange		

Figure 17: A35CHM Motor Information